Rechargeable Batteries

International Edition: DOI: 10.1002/anie.201509564
German Edition: DOI: 10.1002/ange.201509564

VOCl as a Cathode for Rechargeable Chloride Ion Batteries

*Ping Gao, M. Anji Reddy, Xiaoke Mu, Thomas Diemant, Le Zhang, Zhirong Zhao-Karger, Venkata Sai Kiran Chakravadhanula, Oliver Clemens, R. Jürgen Behm, and Maximilian Fichtner**

Abstract: *A novel room temperature rechargeable battery with VOCl cathode, lithium anode, and chloride ion transporting liquid electrolyte is described. The cell is based on the reversible transfer of chloride ions between the two electrodes. The VOCl cathode delivered an initial discharge capacity of 189 mAh g^{-1}. A reversible capacity of 113 mAh g^{-1} was retained even after 100 cycles when cycled at a high current density of 522 mA g^{-1}. Such high cycling stability was achieved in chloride ion batteries for the first time, demonstrating the practicality of the system beyond a proof of concept model. The electrochemical reaction mechanism of the VOCl electrode in the chloride ion cell was investigated in detail by ex situ X-ray diffraction (XRD), infrared spectroscopy (FTIR), transmission electron microscopy (TEM), and X-ray photoelectron spectroscopy (XPS). The results confirm reversible deintercalation–intercalation of chloride ions in the VOCl electrode.*

Recently, a novel rechargeable battery was demonstrated based on a room temperature chloride shuttle.[1] Selected electrochemical couples of this chloride ion battery (CIB) offer theoretical energy densities up to a value of 2500 Wh L^{-1}.[1,2] In principle, various metals with low reduction potential, such as Li, Mg, and Ca, can be used as anode materials for this system. In our previous study, Li and Mg metals were used as anodes for chloride ion battery cells with different cathode materials.[1–4] In the first study of a CIB by Zhao et al.,[1] using $BiCl_3$, VCl_3, and $CoCl_2$ cathodes, proof of principle was demonstrated. These electrodes exhibited an interesting electrochemical performance as rechargeable batteries. Furthermore, metal oxychlorides such as FeOCl, BiOCl, and VOCl, have been proposed as potential cathode materials for CIBs.[2–4] The cathodic and anodic reactions of the CIB during a discharge process can be described as follows:

$$\text{Cathode}: \ \mathrm{MCl}x + x\mathrm{e}^- \leftrightarrow \mathrm{M} + x\mathrm{Cl}^-$$

$$\text{Anode}: \ \mathrm{M}' + x\mathrm{Cl}^- \leftrightarrow \mathrm{M}'\mathrm{Cl}x + x\mathrm{e}^-$$

where the cathode consists of metal (M: Fe, Bi, or V), or metal monoxide (FeO, BiO, or VO), and the anode contains a highly electropositive metal (M′: Li, Mg, or Ca). One issue recognized in the first CIB was dissolution of certain metal chlorides in the electrolyte, which could cause a poor electrochemical performance. Investigation of CIB currently focuses on exploring potential electrodes or electrode combinations with high reversibility, as well as compatible electrolytes. Ionic liquids were used as electrolytes in previous studies, but other non-aqueous electrolytes based on carbonate solvent can also be used in CIBs, as described below. Herein, we report a novel room temperature chloride ion battery (Li/PP_{14}Cl-PC/VOCl) that uses a VOCl electrode as a cathode, lithium metal as an anode, and a solution of 0.5 M 1-butyl-1-methylpiperidinium chloride (PP_{14}Cl) in propylene carbonate (PC) as an electrolyte. The electrochemical results of the Li/PP_{14}Cl-PC/VOCl cell were compared with that of a lithium ion cell built with the same cathode and anode, but with a $LiPF_6$ electrolyte.

VOCl was synthesized by a solid–gas reaction, as described in previous work.[4] Typical synthesis involved heating of a 1:1.8 molar ratio of V_2O_3 (98%, Sigma–Aldrich) and VCl_3 (97%, Sigma–Aldrich) in an evacuated and sealed quartz tube kept at a temperature of 893 K for 120 h with a heating rate of 1 K min^{-1}. The resulting brown VOCl material was washed with water and acetone to remove residual VCl_3. Layered VOCl crystallized in an orthorhombic structure with a space group of *Pmmn* (lattice parameter: a = 3.78 Å, b = 3.30 Å, c = 7.91 Å).[5] The buckled V-O bilayer is sandwiched between chlorine layers that are weakly coupled along lattice vector c by van der Waals forces.[6]

The XRD pattern of the as-synthesized VOCl is given in Figure 1. All peaks matched well with the VOCl reference pattern from PDF card number 01-074-1274. Moreover, we found small amounts of impure phases of V_2O_3 (ca. 2 wt%), VCl_2 (ca. 1 wt%), and presumably an fcc metal, which were found to be unaffected by subsequent discharging–charging cycles (Figure S2, Supporting Information), showing their electrochemical inactivity. The SEM images of as-synthesized VOCl particles are shown in Figure S3 (Supporting Information). They exhibit a rod shape morphology with a length of

[*] P. Gao, Dr. M. A. Reddy, Dr. X. Mu, L. Zhang, Dr. V. S. K. Chakravadhanula, Prof. Dr. R. J. Behm, Prof. Dr. M. Fichtner
Helmholtz Institute Ulm for Electrochemical Energy Storage (HIU)
Helmholtzstrasse 11, 89081 Ulm (Germany)
E-mail: m.fichtner@kit.edu
Dr. X. Mu, Dr. Z. Zhao-Karger, Dr. V. S. K. Chakravadhanula, Dr. O. Clemens, Prof. Dr. M. Fichtner
Institute of Nanotechnology, Karlsruhe Institute of Technology (KIT)
P.O. Box 3640, 76021 Karlsruhe (Germany)
Dr. T. Diemant, Prof. Dr. R. J. Behm
Institute of Surface Chemistry and Catalysis, Ulm University
Albert-Einstein-Allee 47, 89081 Ulm (Germany)
Dr. O. Clemens
Joint Research Laboratory Nanomaterials, University of Technology Jovanka-Bontschits-Strasse 2, 64287 Darmstadt (Germany)

Supporting information for this article can be found under http://dx.doi.org/10.1002/anie.201509564.

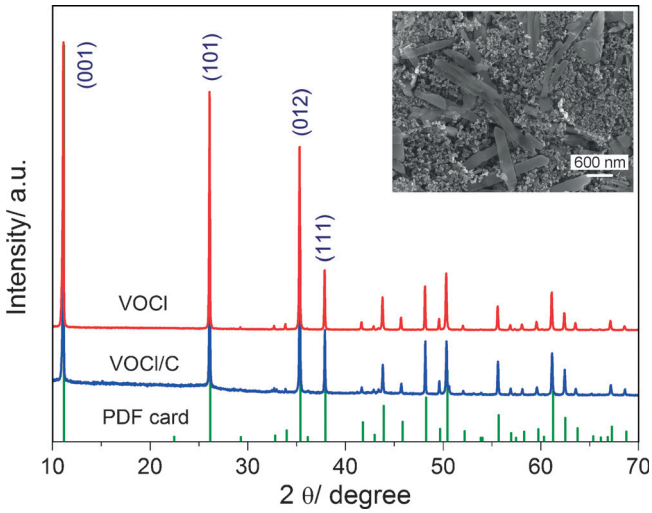

Figure 1. XRD patterns of VOCl and VOCl/C composites, SEM image (inset) of the VOCl/C composite. For a plot of the Rietveld analysis see Figures S1 and S2 (Supporting Information).

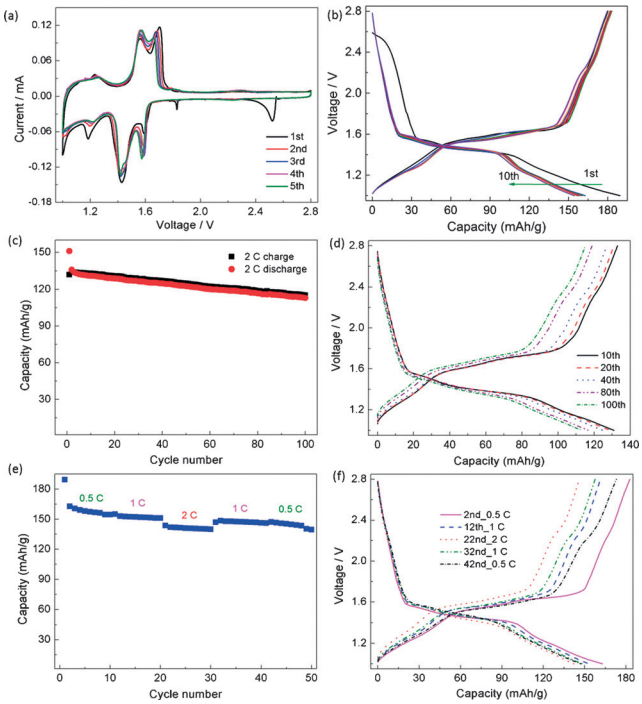

Figure 2. a) CV curves of a Li/PP_{14}Cl-PC/VOCl cell at a scan rate of 0.1 mV s^{-1}; b) initial charge–discharge curves of the cell at 0.5 C in the voltage range 1.0–2.8 V; c) and d) cycling performance at 2 C; e) and f) rate performance of the Li/PP_{14}Cl-PC/VOCl cell.

2–5 μm and approximately 300 nm diameter. VOCl semiconductor[7–9] was mixed with carbon black conducting additive using a mortar and pestle, thereby providing good electrical contact of VOCl in the electrode. The inset in Figure 1 shows that VOCl particles were homogenously dispersed in carbon black, and retained the same morphology and particle size as the pure VOCl material shown in Figure S3 (Supporting Information).

The liquid electrolyte PP_{14}Cl-PC (0.5 M) prepared in this study has a high ionic conductivity of 4.4 mS cm^{-1}, with an electrochemical window of 3.2 V relative to lithium metal measured at room temperature (Figure S4, Supporting Information), which provide a stable environment for electrochemical reaction. The initial CV curves of the Li/PP_{14}Cl-PC/VOCl cell, scanned at 0.1 mV s^{-1} in the voltage range of 1.0–2.8 V and 0.5–3.0 V, are shown in Figure 2 a and Figure S5 (Supporting Information), respectively. Three main redox couples were observed at 1.57/1.67 V, 1.42/1.56 V, and 1.2/1.26 V in a voltage range of 1.0–2.8 V, indicating that a multi-step reaction proceeds during the discharge–recharge process. A structural model for the stepwise behavior of this reaction is proposed in the Supporting Information. First and subsequent CV cycles were similar, which demonstrates the reversibility of the electrochemical process. Additionally, an irreversible anodic peak was observed at around 2.5 V in the first cycle. The origin of this peak is discussed below. Figure 2 b shows the discharge and charge curves of the Li/PP_{14}Cl-PC/VOCl cell for the first 10 cycles, obtained at a rate of 0.5 C (1 C = 261 mA g^{-1}) at 298 K. A small plateau was observed at 2.5 V, followed by a monotonic voltage drop to 1.7 V, and three discharge plateaus at around 1.6, 1.5, and 1.2 V. The corresponding differential capacity plots are shown in Figure S6 (Supporting Information), giving similar peaks as those observed by CV. The cell delivered a total discharge capacity of 189 mAh g^{-1} in the first discharge, corresponding to 0.72 electrons per VOCl unit participating in the reaction. A capacity of 180 mAh g^{-1} was recovered in the first recharge process with an irreversible capacity loss (ICL) of 9 mAh g^{-1} at 0.5 C in the first cycle. Subsequent discharge–charge curves were similar to the first discharge–charge cycle, indicating a high reversibility of the VOCl electrode in this battery.

The length of the small plateau at 2.5 V corresponds to a capacity of 20 mAh g^{-1}, which is equivalent to a 0.07 mol electron transfer. This step is attributed to intercalation of 1-butyl-1-methylpiperidinium ions (PP_{14}^{+}) from the electrolyte into the VOCl electrode. Previous reports indicate that large organic cations can be intercalated into the interlayer of metal oxychlorides.[10–14] The intercalated molecule has in fact been detected by combined XRD, FTIR and XPS measurements, which will be discussed later.

The cycling performance of Li/PP_{14}Cl-PC/VOCl operated at a current density of 2 C is given in Figure 2 c. An initial discharge capacity of 151 mAh g^{-1} was obtained in the voltage range 1.0–2.8 V. Capacity then reduced to 135 mAh g^{-1} in the second cycle and a capacity of 113 mAh g^{-1} was obtained after 100 cycles with a coulombic efficiency of 98 %. Polarization increased slightly during cycling, as shown in Figure 2 d. The rate performance of the Li/PP_{14}Cl-PC/VOCl battery is shown in Figure 2 e. Discharge capacities of 189 mAh g^{-1}, 154 mAh g^{-1}, and 143 mAh g^{-1} were obtained at 0.5 C (first), 1 C (11th), and 2 C (21st) rates, respectively. After 10 cycles at 2 C, the discharge capacity of 148 mAh g^{-1} (1 C, 32nd) and 147 mAh g^{-1} (0.5 C, 42nd) was recovered in subsequent cycling. These results demonstrate that the cell is capable of delivering a high rate capacity and decent cycling stability. The charge–discharge curves of the VOCl electrode cycled at different current densities are presented in Figure 2 f, where

a similar curve with slightly increased polarization was observed at a high current density.

To understand the reaction mechanism of the Li/PP_{14}Cl-PC/VOCl battery, ex situ XRD of the VOCl electrode and lithium anode was performed at different electrochemical states in the first and 10th cycle to investigate phase evolution during electrochemical reaction (Figure 3). Figure 3a shows

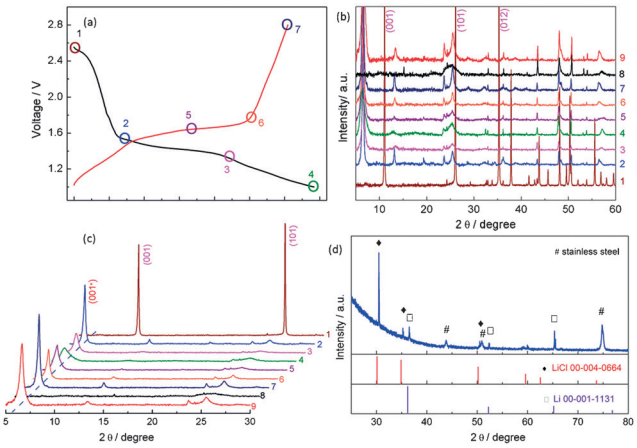

Figure 3. a) Charge–discharge curves of the VOCl electrode at 1 C during the first cycles. The different electrochemical states at which ex situ XRD measurements were performed are marked. b and c) Ex situ XRD patterns of the VOCl electrode at different charge–discharge states during the first and 10th cycles. d) XRD patterns of the lithium anode after the first discharge.

the discharge–charge curve of the VOCl electrode for the first cycle at 1 C with seven discharged and charged states where ex situ XRD measurements were made. In the first cycle, points 1–7 describe the VOCl electrode in various electrochemical states: 1) as-prepared, 2) discharged 1.53 V; 3) discharged 1.33 V; 4) discharged 1.0 V; 5) recharged 1.62 V; 6) recharged 1.75 V; and 7) recharged 2.8 V. Point 8 and 9, shown in Figure 3b and 3c, correspond to the discharged 1.0 V and recharged 2.8 V states of the VOCl electrode in the 10th cycle. Figure 3b shows the full XRD pattern, and Figure 3c displays the selected XRD patterns at low angles. After discharging to 1.53 V (point 2), the XRD pattern was significantly different from that of the as-prepared VOCl electrode, particularly in the low-angle region (Figure 3b,c). A new strong reflection evolved at $2\theta = 6.5°$, which corresponds to a d-spacing value of 13.38 Å. Compared to the original VOCl with a *c* axis spacing of 7.91 Å, a 5.47 Å expansion took place, which indicates intercalation of PP_{14}^+ between the VOCl interlayers during the initial discharge stage. The PP_{14}^+ ion is illustrated in Figure S7 (Supporting Information). It is expected that the ion prefers an orientation horizontal with respect to the host. Expansion of MOCl layers upon intercalation of large organic cations was also noticed in other metal oxychlorides, such as FeOCl,[10–13] TiOCl,[14] and VOCl.[14,15] All further reflections at higher angles strongly decrease in intensity, which is indicative of substantial disorder (potentially resulting from the relative torsion of neighboring layers or buckling of layers; relative reorientation of neighboring layers is a well-known phenomenon of this structure type).[12,16,17] Analysis of the patterns in the charged and discharged states is provided in the Supporting Information. Upon further discharge to points 3 and 4, reflections assigned to the VOCl-type phase show increased broadening. Interestingly, upon recharging to 2.8 V (point 7), the initial width is gradually recovered, demonstrating the topotactic nature of the electrochemical reaction (see Supporting Information for a more detailed explanation). In the discharge state of the 10th cycle (Figure 3b,c, point 8), (00l)-type reflections show an extremely strong increase of broadening, while remaining parts of the pattern are similar to previous charge–discharge states. However, in the subsequent recharge (point 9), all peaks were recovered and the XRD pattern was in good agreement with the pattern recorded in the first cycle (point 7). This observation is in good agreement with the observed topotactic nature of the reaction, and suggests that increasing cycle number has a substantial influence on disorder within the crystalline lattice. In Figure 3c, sharp reflections observed in XRD patterns 2–9 belong to impurity phases that are also found in state 1, but with greater visibility because of a strong decrease of overall intensity (a fit of the diffraction data from point 7 is shown in the Supporting Information, Figure S8).

The lithium anode was also tested by ex situ XRD to further understand phase evolution in the first discharge, as shown in Figure 3d. Reflections at $2\theta = 30.4°$, 35.2°, and 50.3°, related to LiCl (PDF card no. 00-004-0664) were detected, as well as a lithium phase ($2\theta = 36.2°$, 52.1°, and 65.2°; PDF card no. 00-001-1131), and the stainless steel current collector ($2\theta = 43.8°$, 50.9°, and 74.9°). These results demonstrate that the lithium anode was oxidized into LiCl by chloride ions transported through the electrolyte during discharge. The Cl:V ratio, determined from the SEM-EDX spectra measured at several particles on the VOCl electrodes after the first cycle (Figure S9, Supporting Information), indicates a loss and gain of chloride in the discharge and recharge processes, respectively. Taken together, the voltage composition profiles and ex situ XRD results demonstrate that the discharge–charge reaction mechanism in the first and subsequent cycles is the same.

Figure 4a shows a STEM-HAADF overview image of the rod-shape morphology in the as-prepared sample. The HRTEM micrograph (Figure 4b) reveals the layered structure corresponding to the van der Waals bonded $(001)_{VOCl}$ planes. In the discharged state, the HRTEM micrograph (Figure 4d) shows layered features. The corresponding fast Fourier transformation (FFT; Figure 4e) exhibits broad peaks with a 1.2 nm lattice distance, corresponding to a distorted $(001)_{VOCl}$ lattice, in agreement with the XRD results in Figure 3b. Figure S10 (Supporting Information) demonstrates that the discharged sample is sensitive to electron beam damage. Under electron beam irradiation (approximately 5×10^7 electrons nm^{-2}) 2–3 nm vanadium (III) oxide crystallites formed with a space group of $Fm\bar{3}m$ (225).[18] This result indicates the meta-stability of the layered structure in the discharged sample, in contrast with that of the as-prepared and recharged samples. The *d*-values determined from the STEM-HAADF and the HRTEM micrographs of the

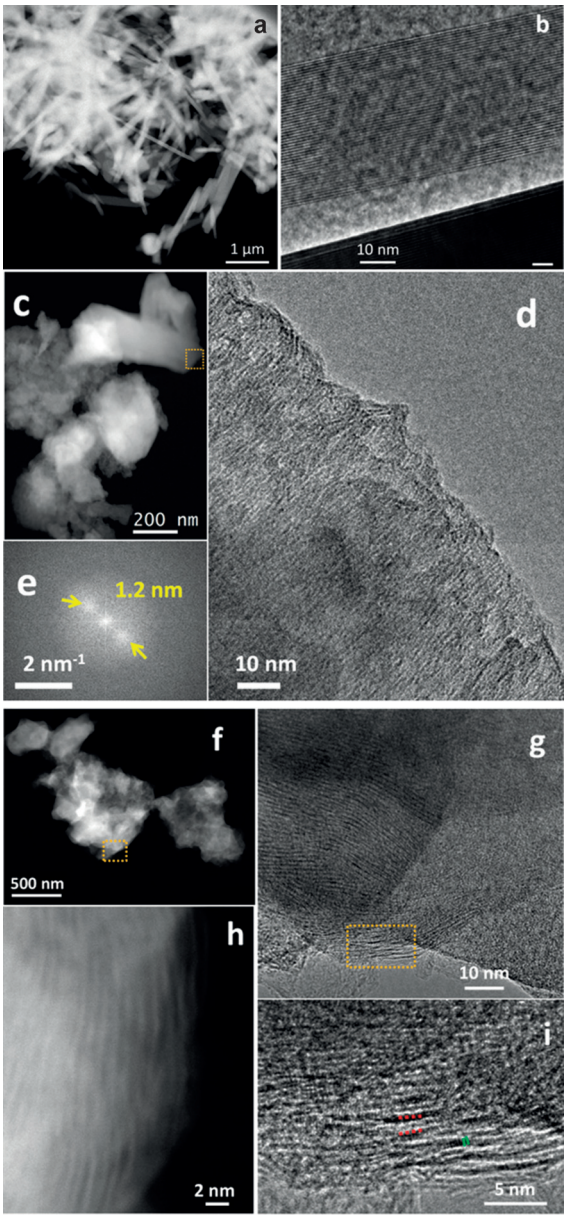

Figure 4. a) STEM-HAADF large-area image; b) enlarged HRTEM micrograph of the as-prepared VOCl; c) STEM-HAADF overview image of the discharged sample; d) low-dose HRTEM micrograph from the area indicated in (c); e) fast Fourier transform of the HRTEM image in (c), where yellow arrows highlight reflections corresponding to $(001)_{VOCl}$; f) STEM-HAADF overview image of the recharged sample; g) HRTEM micrograph from the area indicated in (f); i) magnified image of the marked area in (g), where red dots highlight distorted (001) lattices with a d-value of approximately 1.2 nm; h) STEM-HAADF image from the same area as (i), showing the distorted (001) lattices.

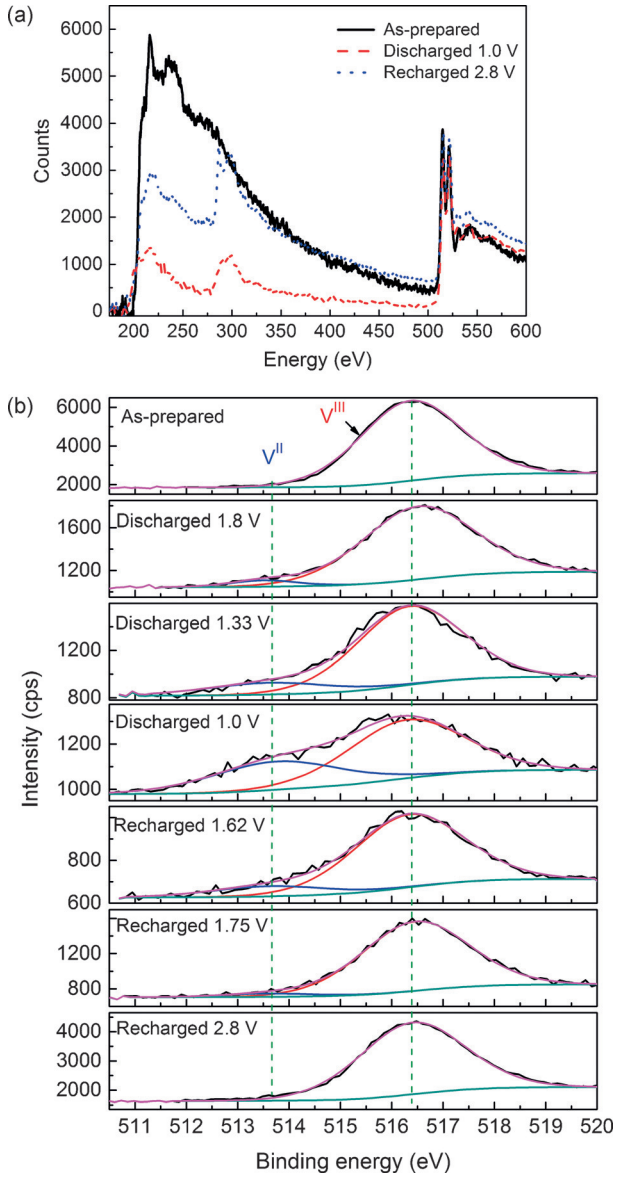

Figure 5. a) EEL spectra of the as-prepared, discharged, and recharged samples. Features at 285 eV correspond to the carbon K-edge of the binder. The spectra are vertically aligned with respect to the background subtracted vanadium peak. b) XPS spectra in the V $2p_{3/2}$ region of VOCl electrodes in various electrochemical states. Line key: experimental data (black); fitted signals (light blue and red); fitted background (green).

recharged sample (Figure 4 g–i) correspond to the distorted reflection of the $(001)_{VOCl}$ lattice plane. TEM mapping of the discharged and recharged VOCl electrodes is shown in Figures S11 and S12 (Supporting Information), respectively. Figure 5 a shows EEL spectra recorded on the same area of the TEM for the as-prepared, discharged, and recharged samples, including the Cl L-edge at 200 eV and the V L-edge at 512 eV. The three background corrected spectra are aligned with respect to the vanadium signal. The area under the Cl L-edge directly relates to the relative amount of Cl in the three samples, implying a loss and gain of chloride ions in the VOCl electrode during the discharge and recharge process, respectively.

The oxidation state of vanadium in different electrochemical states was investigated by ex situ XPS measurements to further understand the reaction mechanism of the $Li/PP_{14}Cl$-PC/VOCl cell. Figure 5 b shows the XPS spectra of the V $2p_{3/2}$ regions in the as-prepared, discharged (1.8 V, 1.33 V, 1.0 V), and recharged (1.62 V, 1.75 V, 2.8 V) states of the VOCl electrode for the first cycle. Survey spectra of the

electrode at these points are provided in Figure S13 (Supporting Information). In the as-prepared sample, a single peak was observed in the V $2p_{3/2}$ region with a binding energy of 516.3 eV, which can be ascribed to trivalent vanadium in VOCl.[19] Upon discharging to 1.8 V, a new peak with a binding energy of 513.7 eV appeared, which is attributed to V^{2+}, as well as the V $2p_{3/2}$ peak at 516.3 eV, which is attributed to the V $2p_{3/2}$ state in V^{3+}.[20] The peak area attributed to V^{2+} (it is not large, which may be because of its sensitivity on the surface) generally increased upon discharge, and decreased again during the recharge process. For XPS spectra corresponding to the recharged VOCl (2.8 V), the lower binding energy peak disappeared and only the peak at 516.3 eV remained, demonstrating that V^{2+} was transformed back into V^{3+} during the recharge process. The observation of vanadium in a lower chemical valence can be ascribed to the partial reduction of V^{3+} into V^{2+}, in accordance with dissociation of chloride ions from VOCl during the discharge process. After recharging, V^{3+} was re-acquired by the VOCl electrode, which demonstrates a reversible oxidation–reduction process. XPS spectra of the Cl 2p region of VOCl electrodes and lithium anodes in different states are shown in Figures S14 and S15 (Supporting Information), respectively.

To gain further insight into the potential intercalation of the organic cation from $PP_{14}Cl$ into VOCl, we performed additional IR, XPS, and SEM measurements. The discharged electrode was washed several times with PC and DMC (dimethyl carbonate), to remove any $PP_{14}Cl$ precipitated on the surface of the electrode. Figure S16 (Supporting Information) shows the FTIR spectra of the PVDF (polyvinylidene fluoride) VOCl after discharge to 1.33 V and $PP_{14}Cl$. Assigned FTIR spectra of the VOCl electrode in different electrochemical states are shown in Figures S17, S18, and Table S1 (Supporting Information). Bands have been assigned at 944 cm^{-1} (N–C (CH_3) stretching and the twisting/rocking of H-C–H in the piperidinium ring), 2872 cm^{-1} (symmetric C–H stretching in the butyl group) and 2938 cm^{-1} (symmetric and asymmetric C–H stretching in the piperidinium ring).[21] A shift of the bands to lower frequencies (921, 2866, and 2920 cm^{-1}) was observed in charged–discharged samples, which is in agreement with analogous layered material intercalated with guest molecules,[16] suggesting intercalation of PP_{14}^+ cations with VOCl interlayers. Figure S19 (Supporting Information) shows the N 1s XPS spectra of the VOCl electrode in the as-prepared, discharged (1.8 V and 1.33 V), and recharged (1.62 V and 1.75 V) states. Appearance of the N 1s peak after discharging to 1.8 V, and its persistence during recharging, further demonstrates intercalation of the PP_{14}^+ cation and VOCl electrode. Moreover, an expansion of the layered structure of the discharged VOCl electrode was also observed by SEM (Figure S20, Supporting Information). Based on the above observations and XRD results, we conclude that PP_{14}^+ is intercalated with the layered VOCl material during the initial stage of the first discharge and remains intercalated during further cycles.

Based on the electrochemical, ex situ XRD, TEM, FTIR, and XPS analyses we postulate the following mechanism for the Li/PP_{14}Cl-PC/VOCl cell. During the initial discharge at 2.5 V, 0.07 mol of PP_{14}^+ was intercalated irreversibly into the VOCl electrode, leading to an expansion of layers. For charge balancing, an equal amount of Cl^- ions reacts with the anode and forms LiCl. Upon further discharge, chloride ions are deintercalated from VOCl, transported through the electrolyte, and react with lithium to form LiCl. During the recharge process chloride ions are intercalated into the VOCl electrode. Intercalated PP_{14}^+ facilitates the chloride deintercalation–intercalation process by keeping layers widely spaced and intact, which is indicated by a reversible change of width of the peak at $2\theta = 6.5°$ during discharging–charging. This could be the reason for the good reversible capacity of the electrode, which is also observed for high current densities. The proposed reaction mechanism and experimental details are outlined in further detail in the Supporting Information.

It is interesting to compare the discharge profiles of the Li/PP_{14}Cl-PC/VOCl and Li/$LiPF_6$-EC-DMC-PC/VOCl cells, the former based on chloride ion transport and the later based on lithium ion transport (Figure S21, Supporting Information). The discharge–charge profiles of the cell based on lithium ion transport are completely different, and give further evidence that the Li/PP_{14}Cl-PC/VOCl cell operates by a different mechanism. By contrast, in the chloride ion cell the discharge product of LiCl may dissolve to a certain extent, even given low solubility in PC solvent. Therefore, the interference arising from intercalation of lithium in the VOCl electrode cannot be ignored during long cycling.

In summary, we have presented a novel room temperature Li/PP_{14}Cl-PC/VOCl chloride ion battery using VOCl as a cathode, lithium foil as an anode, and $PP_{14}Cl$ dissolved in propylene carbonate solvent as the electrolyte. The reversible behavior of the Li/PP_{14}Cl-PC/VOCl cell was characterized by CV and galvanostatic measurements. The results show that the battery can be well discharged and recharged even at a high current density. The cell shows an initial discharge capacity of 189 mAh g^{-1} at 0.5 C, corresponding to 0.72 mol of electrons transferred during reaction. A discharge capacity of 113 mAh g^{-1} was obtained at 2 C with a coulombic efficiency of 98 % over 100 cycles. The mechanism of the Li/PP_{14}Cl-PC/VOCl chloride ion battery was validated by ex situ XRD, TEM, FTIR, and XPS measurements. The results indicate that chloride ions shuttle between cathode and anode.

Acknowledgements

Financial support from China Scholarship Council (CSC; P.G.) and through the EU project Hi-C in FP 7, grant no. 608575 (X.M.), is gratefully acknowledged. The authors thank Nina Laszczynski, Helmholtz Institute Ulm, for the lithium anode XRD measurement and the Karlsruhe Nano Micro Facility (KNMF) for access to a TEM. V.C. and X.M. thank Dr. Christian Kübel and Prof. Dr. Horst Hahn for their continuous support.

Keywords: chloride ion batteries · electrochemistry · rechargeable batteries · vanadium oxychloride

How to cite: *Angew. Chem. Int. Ed.* **2016**, *55*, 4285–4290
Angew. Chem. **2016**, *128*, 4357–4362

[1] X. Zhao, S. Ren, M. Bruns, M. Fichtner, *J. Power Sources* **2014**, *245*, 706 – 711.
[2] X. Zhao, Z. Zhao-Karger, D. Wang, M. Fichtner, *Angew. Chem. Int. Ed.* **2013**, *52*, 13621 – 13624; *Angew. Chem.* **2013**, *125*, 13866 – 13869.
[3] X. Zhao, Q. Li, Z. Zhao-Karger, P. Gao, K. Fink, X. Shen, M. Fichtner, *ACS Appl. Mater. Interfaces* **2014**, *6*, 10997 – 11000.
[4] P. Gao, X. Zhao, Z. Zhao-Karger, T. Diemant, R. J. Behm, M. Fichtner, *ACS Appl. Mater. Interfaces* **2014**, *6*, 22430 – 22435.
[5] H. Schäfer, F. Wartenpfuhl, *J. Less-Common Met.* **1961**, *3*, 29 – 33.
[6] N. A. Bogdanov, J. Van Den Brink, L. Hozoi, *Phys. Rev. B* **2011**, *84*, 235146 – 235146.
[7] S. Glawion, M. Scholz, Y.-Z. Zhang, R. Valentí, T. Saha-Dasgupta, M. Klemm, J. Hemberger, S. Horn, M. Sing, R. Claessen, *Phys. Rev. B* **2009**, *80*, 155119.
[8] E. Benckiser, R. Rückamp, T. Möller, T. Taetz, A. Möller, A. A. Nugroho, T. T. M. Palstra, G. S. Uhrig, M. Grüninger, *New J. Phys.* **2008**, *10*, 053027.
[9] P. Palvadeau, D. Schleich, J. Rouxel, *Mater. Res. Bull.* **1979**, *14*, 891 – 897.
[10] J. F. Bringley, B. A. Averill, *Chem. Mater.* **1990**, *2*, 180 – 186.
[11] J. F. Bringley, J.-M. Fabre, B. A. Averill, *J. Am. Chem. Soc.* **1990**, *112*, 4577 – 4579.
[12] S. M. Kauzlarich, J. L. Stanton, J. Faber, B. A. Averill, *J. Am. Chem. Soc.* **1986**, *108*, 7946 – 7951.
[13] R. H. Herber, Y. Maeda, *Inorg. Chem.* **1981**, *20*, 1409 – 1415.
[14] I. Kargina, D. Richeson, *Chem. Mater.* **1996**, *8*, 480 – 485.
[15] S. Clough, P. Palvadeau, J. P. Venien, *J. Phys. C* **1982**, *15*, 641 – 655.
[16] L. Cario, S. Delagrange, F. Boucher, E. Faulques, P. Palvadeau, *Chem. Mater.* **2003**, *15*, 4325 – 4331.
[17] J. E. Phillips, R. H. Herber, *Inorg. Chem.* **1986**, *25*, 3081 – 3088.
[18] N. Schönberg, W. G. Overend, A. Munthe-Kaas, N. A. Sörensen, *Acta Chem. Scand.* **1954**, *8*, 221 – 225.
[19] M. Demeter, M. Neumann, W. Reichelt, *Surf. Sci.* **2000**, *454 – 456*, 41 – 44.
[20] E. Hryha, E. Rutqvist, L. Nyborg, *Surf. Interface Anal.* **2012**, *44*, 1022 – 1025.
[21] M. Shukla, H. Noothalapati, S. Shigeto, S. Saha, *Vib. Spectrosc.* **2014**, *75*, 107 – 117.

Received: October 12, 2015
Revised: December 22, 2015
Published online: February 29, 2016

